FLUORESCENCE DIFFUSE OPTICAL IMAGE RECONSTRUCTION WITH *A PRIORI* INFORMATION

Lu Zhou, An Jin, Birsen Yazıcı

Rensselaer Polytechnic Institute
110 8th St., Troy, NY 12180

ABSTRACT

This paper addresses fluorescence diffuse optical tomography (FDOT) reconstruction problem with *a priori* information. We assume that approximate location of the fluorophore concentration is known from physiology of the disease and nature of the fluorophore injected. In addition, we assume the anatomical edge structures from an anatomical image modality partially coincident with the edges of the fluorophore concentration image. We formulate FDOT reconstruction in Bayesian framework and model *a priori* information of FDOT into a Gaussian Markov random field (GMRF) with several unknown parameters. We simultaneously estimate the optical image and the unknown *a priori* model parameters. Numerical simulations demonstrate that the *a priori* information could effectively improve the image reconstruction results.

Index Terms— fluorescence, optical tomography, image reconstruction

1. INTRODUCTION

Fluorescence diffuse optical tomography (FDOT) is a rapidly developing functional imaging modality that measures the 3D fluorophore activity inside biological tissue at cellular and molecular level [1]. FDOT requires 3D reconstruction of fluorophore concentration using boundary measurements obtained at the emission and excitation wavelength. However, the nonlinear and ill-posed nature of the FDOT inverse problem makes accurate reconstruction of fluorophore concentration a challenging problem.

Previous studies in the literature showed that incorporating structural *a priori* information from a high resolution imaging modality, such as magnetic resonance imaging (MRI) or X-ray computer tomography (CT), could improve the reconstruction of FDOT images. In [2, 3], the structural *a priori* information from anatomical image is used to decomposes the fluorescence image domain into regions with similar anatomical properties. The reconstruction of fluorophore concentration is constrained spatially to particular segments. This can be considered a as 'hard-constraint' (as defined in [4]). However, it's always possible that the correlation between the *a priori* anatomical image and fluorophore concentration image may not be high. For example, the location of fluorophore concentration in the optical image may not have a corresponding counterpart in the anatomical image. In this case, imposing hard-constraint may lead to erroneous results. Thus the *a priori* information has to be incorporated as a 'soft-constraints' [5] by building a greater degree of uncertainty into the *a priori* model. A study by Davis et al [6] proposed a method to incorporate structural *a priori* information into a Laplacian-type matrix, where the *a priori* information is utilized as a soft-constraint to guide image reconstruction. Although Davis' study added some flexibility to deal with uncertainty in *a priori* information, the improvements in the accuracy of FDOT image reconstruction depends on the assumption of high structural-optical correlation.

In this work, we present an FDOT image reconstruction method where *a priori* information is utilized as a 'soft-constraint' to guide image reconstruction, which can tackle with the case of low structural-optical correlation. We use two types of *a priori* information: (1) The localization information of the fluorophore concentration based on chemical properties of the fluorophore injected and the disease physiology. (2) The anatomical edge structure of the tissue. We build the *a priori* information into Gaussian Markov random field (GMRF) model with several unknown parameters. GMRF has been widely used for modeling spacial images, it captures both localization and edge information of fluorophore concentration. The unknown parameters of GMRF model are estimated iteratively from measurement data, which enables a flexible soft-constraint to guide image reconstruction. In simulation study, we show that when the structural-optical correlation is high, our method can significantly improve the reconstructed image. In addition, even if the correlation is low, our method can still get to good reconstruction results. We compare our method with to Laplacian-type regularization method [6], and show that when the *a priori* structural information deviates from the true optical image, the recon-

This work was supported by U.S. Army Medical Research Acquisition Activity under grant W81XWH-04-1-0559, Center for Subsurface Sensing and Imaging Systems, under the Engineering Research Centers Program of the National Science Foundation under Award Number EEC-9986821.

struction results in our method are much less biased towards the prior as compared to the Laplacian-type regularization technique.

2. FORWARD PROBLEM OF FDOT

We model the forward problem of FDOT in frequency domain. In this work, we assume that the source is time-invariant with zero modulation frequency, which is also known as continuous wave (CW) FDOT. Then the propagation of the excitation and emission light in a bounded domain $\Omega \subset \mathbb{R}^3$ is described by the following coupled diffusion equations:

$$-\nabla \cdot D_x(\boldsymbol{r})\nabla\phi_x(\boldsymbol{r},\boldsymbol{r}_i) + \mu_{ax}(\boldsymbol{r})\phi_x(\boldsymbol{r},\boldsymbol{r}_i) = S_i(\boldsymbol{r}), \quad (1)$$

$$-\nabla\cdot D_m(\boldsymbol{r})\nabla\phi_m(\boldsymbol{r},\boldsymbol{r}_i)+\mu_{am}(\boldsymbol{r})\phi_m(r,\boldsymbol{r}_i) = \phi_x(\boldsymbol{r})\eta\mu_{axf}(\boldsymbol{r}), \quad (2)$$

with the Robin boundary condition

$$2D_{x,m}(\boldsymbol{r})\frac{\partial\phi_{x,m}(\boldsymbol{r},\boldsymbol{r}_i)}{\partial\boldsymbol{n}} + \rho\phi_{x,m}(\boldsymbol{r},\boldsymbol{r}_i) = 0,\ \boldsymbol{r}\in\partial\Omega, \quad (3)$$

where $\phi_{x,m}(\boldsymbol{r},\boldsymbol{r_i})$ is the isotropic photon density of the excitation(emission) light at position $\boldsymbol{r}$ due to the ith point source $S_i(\boldsymbol{r})$ centered at $\boldsymbol{r_i}$. $D_{x,m}(\boldsymbol{r})$ and $\mu_{ax,m}(\boldsymbol{r})$ are diffusion and absorption coefficients of the medium under excitation and emission wavelengths respectively. c is the speed of light propagation in the medium. $\boldsymbol{n}$ is the direction perpendicular to the boundary, and ρ is the boundary mismatch parameter due to the light reflection at the boundary. $\mu_{axf}(\boldsymbol{r})$ is the absorption coefficient of the fluorophore at excitation wavelength, which is related to the fluorophore concentration and is the quantity to be reconstructed. η is the known quantum yield.

In the case of weak fluorophore, it's reasonable to assume that in the NIR spectrum, the contribution of fluorophore absorption to the total absorption is negligible [7]. Thus we make the following simplifying assumptions:

$$\mu_{ax} = \mu_{axe} + \mu_{axf} \approx \mu_{axe} \quad (4)$$

$$\mu_{am} = \mu_{ame} + \mu_{amf} \approx \mu_{ame} \quad (5)$$

where the subscript e denotes endogenous properties and f denotes exogenous properties.

Let $\Gamma_{i,j}$ be the boundary measurement at the jth detector due to the ith source. Using (1)-(3), $\Gamma_{i,j}$ can be modeled as:

$$\Gamma_{i,j} = \int_\Omega g^*(\boldsymbol{r},\boldsymbol{r}_j)\phi_x(\boldsymbol{r},\boldsymbol{r}_i)\eta\mu_{axf}d\boldsymbol{r}, \quad (6)$$

where g^* is the Green's function of adjoint problem associated with (2) [8]. If there are N_s sources, N_d detectors and the total number of measurements is $M = N_s \times N_d$, we can assemble $\Gamma_{i,j}$ into an $M \times 1$ vector as follows:

$$\boldsymbol{\Gamma} = [\Gamma_{1,1},\ldots,\Gamma_{1,N_d},\ldots,\Gamma_{i,j},\ldots,\Gamma_{N_s,N_d}]^T,$$

We discretize the domain into N voxels and let $x_i = \mu_{axf}(\boldsymbol{r}_i)$, where $\boldsymbol{r}_i$ is the center of ith voxel.

$$\boldsymbol{x} = [x_1, x_2, ..., x_N]^T.$$

Discretizing (6) by the finite difference method, we get:

$$\boldsymbol{\Gamma} = Ax, \quad (7)$$

where $A : L^2(\Omega) \to \mathbb{R}^M$ is the vector-valued forward operator.

3. BAYESIAN FDOT IMAGE RECONSTRUCTION WITH GMRF PRIOR MODEL

3.1. GMRF Prior Model

We address the inverse problem within a Bayesian framework. We add zero-mean i.i.d white Gaussian noise ε to the observation model in (7), and obtain:

$$\boldsymbol{\Gamma} = A\boldsymbol{x} + \varepsilon, \quad (8)$$

Thus the data likelihood is given by:

$$p(\boldsymbol{\Gamma}|\boldsymbol{x}) = \frac{1}{(2\pi)^{M/2}\sigma^M}\exp(-\frac{1}{2\sigma_n^2}\|\boldsymbol{\Gamma} - A\boldsymbol{x}\|^2), \quad (9)$$

where σ^2 is the variance of the addictive noise ε.

We model the prior density of $\boldsymbol{x}$ in GMRF as follows:

$$p(\boldsymbol{x}) = \frac{\exp\{U(\boldsymbol{x}|m_k, a_k, b_k^1, b_k^2, b_k^3)\}}{C(m_k, a_k, b_k^1, b_k^2, b_k^3)}, \quad (10)$$

$$U(\boldsymbol{x}|m_k, a_k, b_k^1, b_k^2, b_k^3) = -\sum_k a_k(x_k - m_k)^2 - \sum_k(\sum_{l=1}^3 b_k^l(x_k^l)^2), \quad (11)$$

where $C(\cdot)$ is the partition function, $U(\cdot)$ is known as the Gibbs energy, x_k^l is the difference between kth voxel x_k and its neighboring pixel in the l direction ($l = 1, 2, 3$) in 3D Cartesian coordinate system. $m_k, a_k, b_k^1, b_k^2, b_k^3$ are unknown parameters which vary by location k corresponding to the center of the kth voxel. m_k is the mean value for x_k. a_k penalizes the difference between x_k and m_k. a_k and m_k model fluorophore localization information. b_k^l penalizes the gradient in the l direction. It models fluorophore edge structure across l direction.

Using the *a priori* localization information, we decompose the image domain Ω into foreground R_f and background R_b regions. R_f denotes the pixel locations where fluorophore is expected to accumulate, R_b denotes the pixel locations where no fluorophore is expected. Similarly, for the edge information, we decompose Ω into region R_e^l where fluorophore image is expected to have large gradient in the l

direction, i.e., an edge along the direction perpendicular to the l direction, and R_{ne}^l where no edge perpendicular to the l direction is expected. Next, we assume that m_k, a_k, b_k^l are unknown piece-wise constant functions on the corresponding regions:

$$m_k = \begin{cases} m_f & \boldsymbol{r}_k \in R_f \\ m_b & \boldsymbol{r}_k \in R_b \end{cases}, \quad a_k = \begin{cases} a_f & \boldsymbol{r}_k \in R_f \\ a_b & \boldsymbol{r}_k \in R_b \end{cases},$$

$$b_k^l = \begin{cases} b_e^l & \boldsymbol{r}_k \in R_e^l \\ b_b^l & \boldsymbol{r}_k \in R_{ne}^l \end{cases}, \; l = 1, 2, 3.$$

Let $\boldsymbol{\theta} = [m_f, m_b, a_f, a_b, b_e^1, b_b^1, b_e^2, b_b^2, b_e^3, b_b^3]^T$ denote the unknown parameter vector of the GMRF prior model. The MAP estimate of $\boldsymbol{x}$ can be obtained from the posterior density function of $\boldsymbol{x}$ as a function of $\boldsymbol{\theta}$. Thus,

$$\hat{\boldsymbol{x}} = \arg\max_{\boldsymbol{x}} p(\boldsymbol{\Gamma}|\boldsymbol{x}) p(\boldsymbol{x}) \tag{12}$$

3.2. Parameters estimation

In this section, we estimate the unknown parameters vector $\boldsymbol{\theta}$ from measurements as follows:

$$\boldsymbol{\theta} = \arg\max_{\boldsymbol{\theta}} J(\boldsymbol{\theta}) \triangleq \arg\max_{\boldsymbol{\theta}} E_{\boldsymbol{x}}[\log p(\boldsymbol{\Gamma}, \boldsymbol{x})|\boldsymbol{\Gamma}, \boldsymbol{\theta}]. \tag{13}$$

The optimal parameters for (13) can be found iteratively by the EM algorithm [9]:

$$\begin{aligned} (\boldsymbol{\theta}^{(q+1)}) &= \arg\max_{\boldsymbol{\theta}} E_{\boldsymbol{x}}[\log p(\boldsymbol{\Gamma}, \boldsymbol{x})|\boldsymbol{\Gamma}, \boldsymbol{\theta}^{(q)}] \\ &= \arg\max_{\boldsymbol{\theta}} E_{\boldsymbol{x}}[-\frac{\|\boldsymbol{\Gamma} - A\boldsymbol{x}\|^2}{2\sigma^2} \\ &\quad - \log C(\boldsymbol{\theta}) + U(\boldsymbol{x}|\boldsymbol{\theta})|\boldsymbol{\Gamma}, \boldsymbol{\theta}^{(q)}] \\ &\triangleq \arg\max_{\boldsymbol{\theta}} F(\boldsymbol{\theta}|\boldsymbol{\Gamma}, \boldsymbol{\theta}^{(q)}), \end{aligned} \tag{14}$$

where $\boldsymbol{\theta}^{(q)}$ is the parameters vector estimated at the qth iteration of the EM algorithm. The pseudo code is given in Algorithm 1.

Algorithm 1 The EM algorithm for parameters estimation.

- Initialize parameter $\boldsymbol{\theta}^{(0)}$

while $|\boldsymbol{\theta}^{q+1} - \boldsymbol{\theta}^q| > T_1$(threshold) **and** $J(\boldsymbol{\theta}^{q+1}) > J(\boldsymbol{\theta}^q)$

- Generate samples of $\boldsymbol{x}$ based on posterior pdf with parameter $\boldsymbol{\theta}^{(q)}$, and calculate $J(\boldsymbol{\theta}^q)$
- Start with $\boldsymbol{\theta} = \boldsymbol{\theta}^q$;

while $|\nabla F| > T_2$ (threshold) **and** step size $\Delta > T_2$

- $\boldsymbol{\theta}' \leftarrow \boldsymbol{\theta} + \nabla F(\boldsymbol{\theta}|\boldsymbol{\Gamma}, \boldsymbol{\theta}^{(q)}) \cdot \Delta$

if $F(\boldsymbol{\theta}'|\boldsymbol{\Gamma}, \boldsymbol{\theta}^{(q)}) > F(\boldsymbol{\theta}|\boldsymbol{\Gamma}, \boldsymbol{\theta}^{(q)})$

- $\boldsymbol{\theta} \leftarrow \boldsymbol{\theta}'$

else

- reduce Δ

end

- $\boldsymbol{\theta}^{q+1} \leftarrow \boldsymbol{\theta}$;

end

4. SIMULATION RESULTS

In this section, we simulated the FDOT image reconstruction using a 2-D phantom shown in Figure 1(a). The reconstruction area is a 6cm×6cm square. The origin of the coordinate system is located at the center of this phantom. The optical properties for the phantom are: $\mu_a = 0.05\text{cm}^{-1}$ and $\mu_s' = 8\text{cm}^{-1}$ ($D = 1/3(\mu_a + \mu_s')$). Within the phantom, $c = 2 \times 10^{10}$cm, and on the boundary of phantom, $\rho = 0.5$. The fluorophore with $\mu_{af} = 0.005\text{cm}^{-1}$ and $\eta = 0.05$ is in a 1.2×1.2 cm square-shaped region, and the center of this region is located at $(-1.20, 0)$. We place 20 sources (black triangles) and 25 detectors (hollow diamonds) on the boundary as shown in Figure 1(a). We add 10% i.i.d. Gaussian noise into the boundary data.

The *a priori* information used in the simulation is presented in Figure 1(b). The 1.2cm×1.2cm shaded area indicates the *a priori* foreground R_f, and the blank area indicates the *a priori* background R_b. R_e^l, $l = 1, 2$, corresponds to the edges of R_f, and R_{ne}^l, $l = 1, 2$, is the the region where no edge is expected across l direction. As we move R_f (shown in Figure 1(b)), the *a priori* localization and edge information deviates from the true corresponding information in the fluorophore concentration image.

Figures 2(a)- 2(c) show the reconstruction results when the *a priori* foreground region is centered at $(-1.2, 0)$, $(-0.3, 0)$ and $(0.3, 0)$, respectively. For comparison, we reconstructed the fluorophore concentration using the Laplacian type regularization [6], which is shown in Figures 2(d)- 2(f), respectively. We observe that in Figure 2(a) and Figure 2(d), where the structural-optical correlation is high, both methods obtain good reconstruction results. However, when the *a priori* information deviates from the true fluorophore concentration image, the images reconstructed by our approach (shown in Figure 2(b) and Figure 2(c)) are less biased towards the prior as compared to the ones reconstructed by the Laplacian-type regularization approach as shown in Figure 2(e) and Figure 2(f).

To evaluate the results quantitatively, we calculate the contrast-to-background noise ratio (CBNR) and the contrast-to-object noise ratio (CONR) of the reconstructed image and summarized them in Table1. The quantitative result is consistent with the visual result presented in Figure 2.

5. CONCLUSION

In this work, we formulated *a priori* information of FDOT by a GMRF model with unknown parameters. These parameters capture *a priori* information on the location and the gradient of fluorophore concentration. We estimated the unknown *a priori* model parameters from measurements using the EM

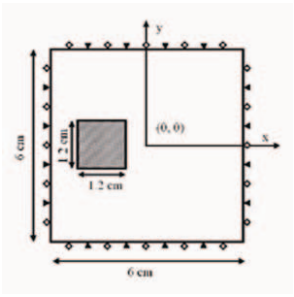

(a) The simulation setup.

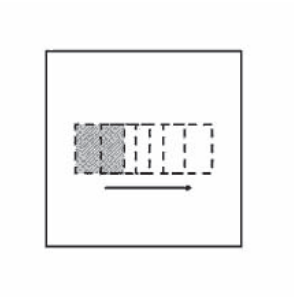

(b) The prior structural image.

Fig. 1. The simulation setup and prior structural image.

Table 1. CBNR and CONR of the reconstruction images in simulation.

R_f center	CBNR		CONR	
	Proposed	Lapalcian	Proposed	Laplacian
(-1.2,0.0)	26.46	29.00	10.35	27.70
(-0.3,0.0)	7.177	4.478	4.744	3.513
(0.3,0.0)	7.639	4.735	3.806	2.352

algorithm. Numerical results show that GMRF model is robust with respect to imperfect *a priori* information. The future work will include applying this algorithm to real phantom or clinical data.

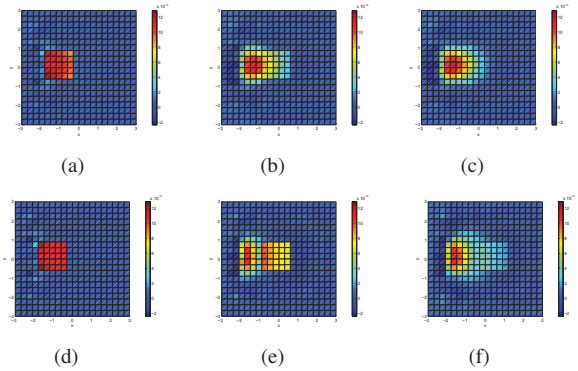

(a) (b) (c) (d) (e) (f)

Fig. 2. (a), (b) and (c) are images reconstructed using the proposed algorithm with expected foreground centered at $(-1.2, 0)$, $(-0.3, 0)$ and $(0.3, 0)$ respectively. (d), (e) and (f) are images reconstructed using the Laplacian type regularization with expected foreground centered at $(-1.2, 0)$, $(-0.3, 0)$ and $(0.3, 0)$ respectively.

6. REFERENCES

[1] V. Ntziachristos, "Fluorescence molecular imaging," *Annu. Rev. Biomed. Eng*, vol. 8, pp. 1–33, 2006.

[2] W. Cong, G. Wang, D. Kumar, Y. Liu, M. Jiang, L. Wang, E. Hoffman, G. McLennan, P. McCray, J. Zabner, and A.Cong, "Practical reconstruction method for bioluminescence tomography," *Optics Express*, vol. 13(18), pp. 6756–6771, 2003.

[3] Y. Lin, H. Gao, O. Nalcioglu, and G. Gulsen, "Fluorescence diffuse optical tomography with functional and anatomical a priori information: feasibility study," *Phys. Med. Biol*, vol. 52, pp. 5569–5585, 2007.

[4] H. Dehghani, B.W. Pogue, J. Shudong, B. Brooksby, and K.D. Paulsen, "Three-dimensional optical tomography: resolution in small-object imaging," *Appl. Opt.*, vol. 42, pp. 3117–3126, 2003.

[5] P.K. Yalavarthy, B.W. Pogue, H. Dehghani, C.M. Carpenter, S. Jiang, and K.D. Paulsen, "Structural information within regularization matrices improves near infrared diffuse optical tomography," *Optics Express*, vol. 15, pp. 8043–8058, 2007.

[6] S.C. Davis, H. Dehghani, J. Wang, S. Jiang, B.W. Pogue, and K.D. Paulsen, "Image-guided diffuse optical fluorescence tomography implemented with laplacian-type regularization," *Optics Express*, vol. 15, pp. 4066–4082, 2007.

[7] V. Ntziachristos and R. Weissleder, "Experimental three-dimensional fluorescence reconstruction of diffuse media by use of a normalized born approximation," *Optics Letters*, vol. 26(12), pp. 893–895, 2001.

[8] S.R. Arridge, "Optical tomography in medical imaging," *Inverse Problem*, vol. 15, pp. R41–R93, 1999.

[9] C.A. Bouman S. Saquib and K. Sauer, "Ml parameter estimation for markov random fields with applications to bayesian tomography," *IEEE Transactions on image processing*, vol. 7, pp. 1029–1044, 1998.